ESTIMATION OF AGGLOMERATE SIZE OF MULTI-WALLED CARBON NANOTUBES IN GAS-SOLID FLUIDIZED BEDS

Sung Woo Jeong[1,2], Jimin Kim[3], Dong Hyun Lee[1*]

[1]*School of Chemical Engineering, Sungkyunkwan University, Seobu-ro 2066, Jangan, Suwon, Gyeonggi, Korea*

[2]*Korea Research Institute of Chemical Technology, Gajeong-ro 141, Yuseong, Daejeon, Korea*

[3]*Catalyst Process R&D Center, SK Innovation, Republic of Korea*

*Email: *dhlee@skku.edu*

Abstract – The hydrodynamic characteristics of multi-walled carbon nanotube agglomerates were investigated using the bed collapse technique and their agglomerate size was determined using the sedimentation method. The bed collapsing process of multi-walled carbon nanotube agglomerates was closer to the Geldart group C particles than to the group A particles. The median diameters of the Multiwall Carbon Nanotubes (MWCNT) agglomerates, determined by sedimentation at an initial superficial gas velocity of 0.120 and 0.190 m/s, were 157 and 221 μm, respectively. The size of the multi-walled carbon nanotube agglomerates in the fluidization state was measured by image analysis using a high speed camera. The median diameter of the multi-walled carbon nanotube agglomerates in the freeboard was increased from 138 to 189 μm as the superficial gas velocity increased from 0.088 to 0.190 m/s at a static bed height of 0.16 m. The median diameter and size distribution determined from the sedimentation fitted well with those measured using image analysis. In this study, the results were reasonable up to a superficial gas velocity of 0.190 m/s.

INTRODUCTION

Geldart (1973) have classified particles based on the mean diameter of the particles and the density difference between the particles and gas. According to Geldart classification, nanoparticles in a gas-solid fluidization belong to group C particles. Geldart group C particles are difficult to fluidize due to their small size and strong cohesive force. However, some researchers, Chaouki et al. (1985), Wang et al. (2002), and Zhu et al. (2005), have reported that nanoparticles can be fluidized in the form of agglomerates. The behavior of agglomerates in the fluidized beds can be divided into two types: agglomerate particulate fluidization (APF) and agglomerate bubbling fluidization (ABF). Wang et al. (2002) reported that fluidization characteristics are influenced by the density and size of the multi-agglomerate structure.

However, it is difficult to analyze the size of particles that have a strong cohesive force such as those of Geldart group C. In addition, agglomerate size in the fluidization state differs from that obtained by size analysis because larger agglomerates are formed in the fluidized beds. While studies on developing a model to predict the size of agglomerates have been carried out by Castellanos (2005), Chaouki et al. (1985), Iwadate and Horio (1998), Morooka et al. (1988), and Zhou and Li (1999), a model applicable to various fluidized beds has not been suggested due to the differences in the properties of agglomerates and the fluidized bed. Studies have also been carried out on modeling to predict the fluidization characteristic and agglomerate size of nano-materials in which the morphology of the primary particle is a spherical particle such as SiO_2 and TiO_2.

In gas-solid fluidized beds, Nam et al. (2004), Wang et al. (2006a), Wang et al. (2006b), Wang et al. (2007), Weber and Mei (2013), Yu et al. (2006), and Zhu et al. (2001) have used intrusive and non-intrusive techniques to measure the hydrodynamics and agglomerate size. While intrusive techniques including optical probing, capacitance probing, thermal probing, and momentum probing have advantages such as low cost and easy installation, they disturb the local behavior of particles. Non-intrusive techniques include various tomography techniques, nuclear magnetic resonance (NMR), and digital image analysis (DIAT). These techniques do not affect the flow of particles and can measure the fluidization behavior of a wide range. However, most non-intrusive techniques are expensive and involve difficult installation. In numerous studies, Nam et al. (2004), Wang et al. (2006a), Wang et al. (2006b), and Wang et al. (2007) have used image analysis to measure the agglomerate size in the fluidized beds because it can be easily installed and is less expensive than the other non-intrusive techniques.

For characterizing particles and the dense phase in the bubbling fluidized bed, Abrahamsen and Geldart (1980), Barreto et al. (1983), Barreto et al. (1988), Chen and Weinstein (1994), Dry et al. (1983), Geldart and Wong (1985), Morooka et al. (1988), Park et al. (1991), Tung and Kwauk (1982), and Yang et al. (1985) have mainly used the bed collapse technique. The bed collapsing process generally involves three stages as

follows: bubble escape stage, hindered sedimentation stage, and solids consolidation stage. According to Yang et al. (1985), the bed collapsing process of the Geldart group A particles involves all three stages, while for the group B particles, the process only involves the bubble escape stage. The bed collapsing process for the group C particles involves both the short hindered sedimentation stage and the long solid consolidation stage. While the results of the bed collapsing process of groups A and B particles are similar in most of the literature, some differences are observed in the interpretation of the bed collapse characteristics for group C particles. Geldart and Wong (1985) have reported that gases escape from the bed in the form of channeling with time because, for the fluidization of group C particles, cavities occur in the bed instead of bubbles. This process is similar to the solid consolidation stage for the Geldart group A particles and proceeds at a slow rate.

In this study, the hydrodynamic characteristics of Multiwall Carbon Nanotubes (MWCNT) agglomerates were investigated using the bed collapse technique, and agglomerate size was determined from sedimentation using the results in the hindered sedimentation stage in which the bed surface was settled at a constant rate. In addition, the sizes of the MWCNT agglomerates were measured in the freeboard using a high speed camera. The result was then compared with the agglomerate sizes determined from sedimentation.

EXPERIMENT

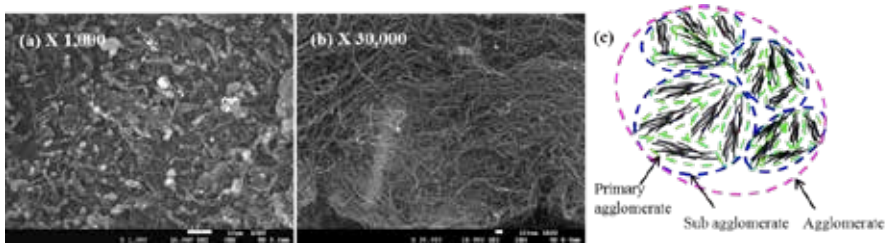

Fig. 1. SEM image of MWCNT agglomerates (a,b) and scheme of multi-agglomerate structure for MWCNT agglomerates (c).

The morphology of the MWCNT agglomerates used in this study is shown in Figs. 1a and 1b. The MWCNT agglomerates have irregular shapes such as elongated shapes and a curled up ball, as can be seen in Fig. 1a. Fig. 1b confirms that the strands of the MWCNTs were entangled with each other. Based on the observations from the SEM image, the scheme of the structure of the MWCNT agglomerates used in this study is shown in Fig. 1c. According to Yu et al. (2003), the strands of the MWCNTs become entangled with each other during the growth of the MWCNTs, and the primary agglomerates are then formed. At the same time, fine primary agglomerates are aggregated in the form of sub-agglomerates, as can be seen in Fig. 1a. Wang et al. (2002) have reported that these sub-agglomerates become larger agglomerates in the fluidized bed. The bulk density (ρ_b) of the MWCNT agglomerates is 20 kg/m^3 due to the multi-agglomerate structure which has significant voidage. The particle density (ρ_s) is 151 kg/m^3, as analyzed by a mercury porosimeter.

Fig. 2 shows a schematic diagram of the experimental apparatus to investigate the characteristics of the MWCNT agglomerates. The MWCNT agglomerates are fluidized in a Plexiglas column. The inside diameter and total height of the column are 0.14 m and 2.4 m, respectively. An expanded column of 0.3 m was placed at the top of the column to reduce the elutriation of particles. The elutriated particles were collected in a cyclone and returned to the column through the

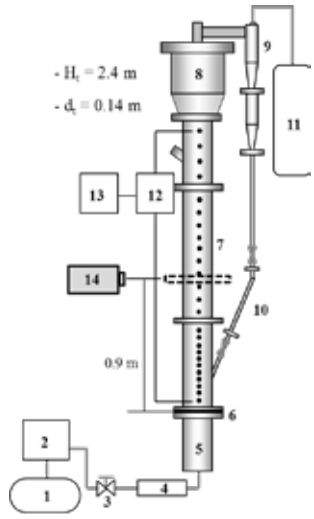

Fig. 2. Schematic diagram of experimental setup; 1 air compressor, 2 air dryer, 3. Pressure regulator, 4 mass flow controller, 5 windbox, 6 distributor, 7 fluidized bed, 8 expansion column, 9 cyclone, 10 standpipe, 11 bag filter, 12 pressure transducer, 13 recorder, 14 high speed camera.

Table 1 Static bed conditions used to measure the size of MWCNT agglomerates in the freeboard.

Initial bed weight; W_0 [kg]	0.053	0.049	0.042
Initial bed height; H_0 [m]	0.172	0.160	0.138

standpipe. A porous plate was used as the gas distributor. Fluidizing gas was introduced into the column using a mass flow controller (MFC). The first port was 0.05 m above the gas distribution for measuring the pressure drop. Ports were placed at intervals of 0.05 m up to 0.55 m. Above the height of 0.55 m, the ports were placed at intervals of 0.10 m. Bed material of 0.09 kg was loaded to measure the pressure drop according to axial height. The static bed height was 0.29 m.

To observe the behavior and measure the size of the MWCNT agglomerates, a high speed camera (Phantom V310; Vision Research Inc.) was installed at the height of 0.9 m above the gas distributor. The light emitted from the LED light source (120 W) passed through the slit (2 x 50 mm) and illuminated the center of the column. The resolution, sample rate, and exposure time of the high speed camera were 1280 pixels X 1024 pixels, 500 frame/s, and 1000 μs, respectively. The static bed conditions are shown in Table 1. The sizes of the MWCNT agglomerates in the freeboard were measured with the superficial gas velocity of 0.088, 0.140, 0.190, and 0.220 m/s at each static bed condition.

The characteristics of the MWCNT agglomerates were investigated using the bed collapse technique. In addition, the size of the MWCNT agglomerates was estimated using data in the hindered sedimentation stage. 0.07 kg of the MWCNT agglomerates was loaded into the column. The MWCNT agglomerates were then fluidized by supplying the fluidizing gas as the air. The bed collapse was initiated by instantaneously disrupting the injection of gas at the fluidization state. After recording the behavior of the bed using the bed collapsing process, the bed height was measured at 1 s intervals using image analysis.

RESULTS AND DISCUSSION

The pressure drop across the bed and the bed height can be determined by measuring the pressure drop with an axial height at a certain superficial gas velocity. Based on the experimental results, the fluidization behavior of the MWCNT agglomerates with a superficial gas velocity was similar to that of the Geldart group A particles. More specific information on the fluidization of MWCNT agglomerates with a superficial gas velocity can be found in the (Jeong et al., 2016).

The solid volume fraction (ε_s) with an axial height can then be calculated by substituting the values in equation (1).

$$-\Delta p_b = H_f\left(1-\varepsilon_g\right)\left(\rho_s-\rho_g\right)g \tag{1}$$

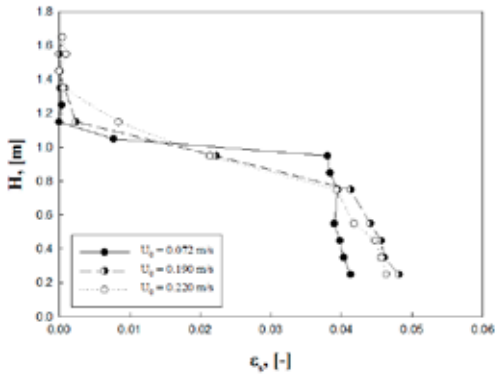

Fig. 3. Solid volume fraction of MWCNT agglomerates with axial height at U_0 = 0.072, 0.190, and 0.220 m/s.

Fig. 3 shows the solid volume fraction (ε_s) with an axial height at the superficial gas velocities of 0.072, 0.190, and 0.220 m/s. Compared with the solid volume fraction of the general particles used in the bubbling fluidized bed, the solid volume fraction of the MWCNT agglomerates was lower than 0.05; this is because the MWCNT agglomerates have a multi-agglomerate structure that has considerable voidage. For the superficial gas velocity of 0.072 m/s, the constant level of solid volume fraction was maintained up to a height of about 1 m. The height of the MWCNT agglomerates was barely greater than 1m. The bed height was determined by measuring the pressure drop according to the axial height and was 0.968 m. This is a typical profile of a solid volume fraction for particulate fluidization. Compared with the case where the

superficial gas velocity was 0.072 m/s, the solid volume fraction in the bed was high and the bed height was low at the superficial gas velocities of 0.190 and 0.220 m/s. For this superficial gas velocity corresponding to the bubbling fluidization regime, the solid volume fraction in the freeboard increased due to the eruption of the MWCNT agglomerates.

The sizes of the MWCNT agglomerates in the freeboard were measured using a high speed camera.

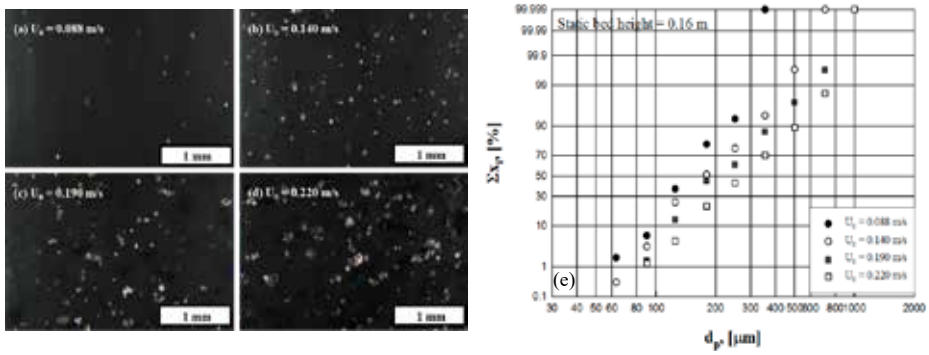

Fig. 4. (a-d) Photograph of MWCNT agglomerates (bright spots) in freeboard measured using high-speed camera; (a) U_0 = 0.088 m/s, (b) U_0 = 0.140 m/s, (c) U_0 = 0.190 m/s, (d) U_0 = 0.220 m/s; (e) Cumulative size distribution of MWCNT agglomerates in the freeboard measured using a camera.

Fig. 4a-d shows a photograph of the MWCNT agglomerates measured using a high speed camera at the height of 0.9 m from the gas distributor with a superficial gas velocity (0.088, 0.140, 0.190, and 0.220 m/s). The static bed height was 0.16 m, and the height of the fluidized bed was 0.45 m at the superficial gas velocity of 0.190 m/s. This means that the MWCNT agglomerates were fluidized in the freeboard. With the light passing through the slit, bright spots were observed, indicating the MWCNT agglomerates as shown in Fig. 4. As the superficial gas velocity was increased from 0.088 to 0.220 m/s, the solid hold-up and fraction of the large MWCNT agglomerates increased in the freeboard. Fig. 4e shows the cumulative size distribution of MWCNT agglomerates measured using a high speed camera at each superficial gas velocity. The initial static bed height was 0.160 m. The measured frequencies of the MWCNT agglomerates were 111, 312, 304, and 401 at the superficial gas velocities of 0.088, 0.140, 0.190, and 0.220 m/s, respectively. The fraction of large agglomerates increased with the increasing superficial gas velocity. This tendency will be discussed later.

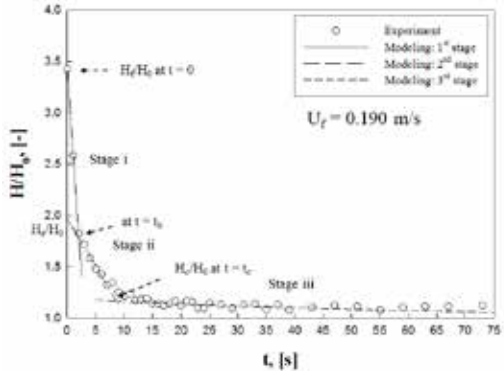

Fig. 5. Bed collapse curve for the MWCNT agglomerates; U_f = 0.190 m/s.

Fig. 5 shows the bed collapse curve of the MWCNT agglomerates. The experimental data fitted well with the curve calculated by the model. The bed collapsing process involved three stages for the MWCNT agglomerates. t_b and t_c, which represent the end of the bubble escape stage and the hindered sedimentation stage, respectively, were 2.03 and 8.62 s, respectively. As shown in Fig. 5, the time for the solid consolidation stage was longer than that for the hindered sedimentation stage. Yang et al. (1985) have wrote that the critical time (t_c) was reduced for fine particles having a strong cohesive force, since the remaining gases between the particles escaped immediately while the agglomerates were rapidly forming. However, the quantitative criteria for discriminating between the group C and group A particles according to the characteristic of bed collapse were unclear. Geldart and Wong (1985) have reported that the bed collapsing process for the Geldart group C particles was similar to the solid consolidation stage for the Geldart group A particles since no bubbles occurred and the bed was expanded due to cavities. For the Geldart group C particles, although quantitative analysis was difficult because research on the characteristic of the bed collapsing process was insufficient, the qualitative features mean that the bed collapsing process of the MWCNT agglomerates is similar to that of the Geldart group C particles.

Determining the particle size by sedimentation is based on Stokes law, whereby the terminal velocity (U_t) of a particle in a fluid is proportional to the particle size. The terminal velocity of a particle can be expressed using Stokes law.

$$U_t = \frac{g d_p^2 (\rho_s - \rho_g)}{18\mu} = \frac{h}{t} \tag{2}$$

The settling velocity and particle size can be calculated by measuring the settling time of any distance. The determined particle size corresponds to the Stokes diameter, which is considered in spherical particles.

According to Chen and Weinstein (1994), the sedimentation of MWCNT agglomerates can be considered as reflecting Stokes flow because the density of the MWCNT agglomerates is very low, and the bed collapse rate is very slow in the hindered sedimentation stage.

Terminal velocity in the Stokes regime is expressed as equation (2). Therefore, particle size (d_p) can be determined from the following equation:

$$d_p = \sqrt{\frac{18\mu h}{g(\rho_s - \rho_f)t}} \tag{3}$$

where h is the bed height with time in the bed collapsing process and refers to the difference between H_f and H as shown in Fig. 5.

According to Deshpande and Telang (1950) and Jiang et al. (2010), for measuring the weight of the settled particles with time, the particle size distribution can be determined from the calculated particle size. In this study, the weight fraction was determined using the variation of the bed height in the bed collapsing process instead of directly measuring the weight. In the sedimentation, the concentration of particles decreased with time. This is because, as the size of the particles increased, they piled up on the bottom of the bed more rapidly. Therefore, the weight fraction of the particles can be expressed as a function of bed height.

$$x_{i,under} = \frac{\varepsilon_i}{\varepsilon_0} = \frac{H_f - H}{H_f} \tag{4}$$

where $x_{i,under}$ is the weight fraction of a particle under the size i, corresponding to the size determined in equation (4).

The results calculated from the collapsing bed, which was initially fluidized at a superficial gas velocity of 0.190 m/s, are shown in Table 2. The median diameter (d_{50}) of the MWCNT agglomerates was 221 μm. Therefore, $Ar^{1/3}$ was calculated as 3.86. However, $Ar^{1/3}$ should be lower than 2.6 to meet the criteria of Stokes law. This means that some deviation exists in the initial assumption.

Table 2. Particle size and cumulative mass fraction at different times using sedimentation method.

t [s]	d_p [μm]	Σx_i
2	201	42.7
3	169	20.5
4	152	17.4
5	140	13.5
6	129	10.5
7	123	9.0

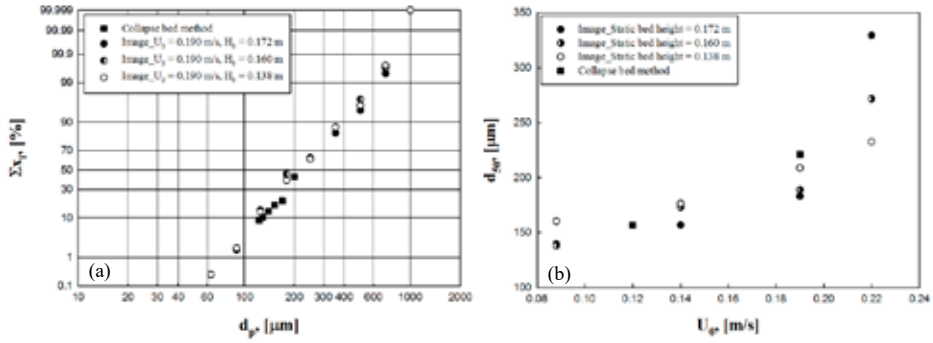

Fig. 6. (a) cumulative size distribution of MWCNT agglomerates obtained by collapse bed method and image analysis, (b) median diameter (d_{50}) of MWCNT agglomerates determined by the image analysis and collapse bed methods.

Fig. 6a shows the cumulative particle size distribution determined by sedimentation and image analysis. It was confirmed that the cumulative particle size distributions that were obtained by sedimentation and image analysis concur, as shown in Fig. 6a. This means that the size determination of the MWCNT agglomerates by sedimentation is reasonable, although the range of particle size distribution determined by sedimentation is limited. Fig. 6b shows the median diameters of the MWCNT agglomerates determined using sedimentation and image analysis with a superficial gas velocity. The median diameters of the MWCNT agglomerates tend to increase with the increasing superficial gas velocity. And the size of the agglomerates that erupted onto the freeboard is influenced by the conflicting factors according to the superficial gas velocity. The first factor is the entrainment of the larger MWCNT agglomerates with the increasing superficial gas velocity due to the enhancement of drag forces acting on the agglomerate. The second factor is the reduction of agglomerate size in the freeboard with the increasing superficial gas velocity, due to the enhancement of external forces such as shear force and collision force. More specific discussion on these factors can be found in (Iwadate and Horio, 1998, Kiani et al., 2013, Matsuda et al., 20004, Morooka et al., 1988, and Zhou and Li, 1999). For the bubbling fluidization of the MWCNT agglomerates, the effect of drag force was more dominant than the effect of size reduction due to external forces because the density was very low and the superficial gas velocity was low for the bubbling fluidization. While the median diameters had similar values of superficial gas velocity in the range from 0.088 to 0.190 m/s, irrespective of static bed height, they clearly increased with the increasing static bed height at a superficial gas velocity of 0.220 m/s. This is due to the increase of the splash zone located between the dense phase and the lean phase according to the superficial gas velocity. The splash zone was composed of erupted particles from the bed and falling particles. As the entrained particle sizes and maximum heights that can be reached were increased by increasing the superficial gas velocity, the splash zone expanded. Compared with the case in which the superficial gas velocity was 0.190 m/s, the solid volume fraction (ε_s) in the bed was lower, although the solid volume fraction (ε_s) in the freeboard was higher at the superficial gas velocity of 0.220 m/s as shown in Fig. 3. Since the momentum which caused the MWCNT agglomerates to erupt is large at 0.220 m/s, the solid volume fraction was precisely increased at the height of 0.9 m with the increasing static bed condition. The difference between the median diameter of the MWCNT agglomerates determined by sedimentation and image analysis was reduced with the decreasing superficial gas velocity. This means that the reliability of the median diameter determined by sedimentation increased, reaching close to the stoke regime. In this study, the results were reasonable up to the superficial gas velocity of 0.190 m/s.

CONCLUSIONS

The solid volume fraction of MWCNT agglomerates with an axial height was determined in a fluidized bed with a diameter of 0.14 m and total height of 2.4 m. The solid volume fraction of the MWCNT agglomerates was lower than 0.05 due to the low density and high bed expansion ratio. The typical solid volume fraction profile of particulate fluidization was measured at the superficial gas velocity of 0.072 m/s. Compared with the case in which the superficial gas velocity was 0.072 m/s, the solid volume fraction in the bed was high and the bed height was low for the case of superficial gas velocities of 0.190 and 0.220 m/s, corresponding to the bubbling fluidization regime.

The bed collapsing process of the MWCNT agglomerates was closer to group C particles than to group A particles. The agglomerate sizes were estimated using the data in the hindered sedimentation stage. The median diameters of the MWCNT agglomerates were determined by sedimentation at the initial superficial gas velocities of 0.120 and 0.190 m/s and were 157 and 221 μm, respectively.

The sizes of the MWCNT agglomerates in the fluidization state were measured using image analysis with a high speed camera. The median diameter (d_{50}) of the MWCNT agglomerates in the freeboard increased from 138 to 189 μm as the superficial gas velocity increased from 0.088 to 0.190 m/s, respectively, at a static bed height of 0.16 m. While no effect was observed of the static bed height on the sizes of the MWCNT agglomerates measured at a height of 0.9 m from the gas distributor to the superficial gas velocity of 0.190 m/s, the sizes of the MWCNT agglomerates increased with the increasing height of the initial static bed at the superficial gas velocity of 0.220 m/s.

The median diameter and size distribution determined from the sedimentation are similar to those measured using the image analysis. The difference between the median diameters of the MWCNT agglomerates determined using sedimentation and those using image analysis increased with the increasing superficial gas velocity. In this study, the results were reasonable up to a superficial gas velocity of 0.190 m/s.

ACKNOWLEDGEMENT

This study was funded by SK Innovation Co., Ltd., Korea. This work was partly supported by the Gyeonggi Regional Research Center (GRRC) program [S-2012-1239-007] of Gyeonggi Province.

NOTATION

d_{50}	median diameter, μm	t_c	time at critical point, s
d_t	diameter of reactor, m	t_b	time when all bubbles have escaped, s
d_p	particle diameter, μm	U_0	superficial gas velocity, m/s
g	acceleration of gravity, m/s^2	U_t	terminal velocity, m/s
H	height of fluidized bed at the ambient condition, m	W_0	initial bed weight, kg
		x_i	mass fraction of solid of size i, -
H_0	static height of initial bed at the ambient condition, m	Δp_b	pressure drop across the bed, Pa
		ε_c	voidage for dense phase, -
H_c	bed height at critical point, m	ε_g	gas voidage, -
H_c	bed height corresponding to dense phase in the bubbling fluidized bed, m	ε_s	solid volume fraction, -
		μ	gas viscosity, Pa·s
H_f	initial bed height for bed collapsing process, m	ρ_b	bulk density, kg/m^3
		ρ_g	gas density, kg/m^3
H_t	height of reactor, m	ρ_s	particle density, kg/m^3
t	run time for bed collapsing process, s		

REFERENCES

Abrahamsen, A.R. Geldart, D. 1980. Behaviour of Gas-Fluidized Beds of Fine powders: Part II. Voidage of the Dense Phase in Bubbling Beds, Powder Technology 26, 47-55.

Barreto, G.F. Mazza, G.D. Yates, J.G. 1988. The Significance of Bed Collapse Experiments in the Characterization of Fluidized Beds of Fine Powders, Chemical Engineering Science 43, 3037-3047.

Barreto, G.F. Yates, J.G. Rowe, P.N. 1983. The Measurement of emulsion Phase Voidage in Gas Fluidized Beds of Fine Powders, Chemical Engineering Science 38, 345-350.

Castellanos, A. 2005. The relationship between attractive interparticle forces and bulk behaviour in dry and uncharged fine powders, Advances in Physics 54, 263-376.

Chen, L. Weinstein, H. 1994. Measurement of Normal Stress and Hindrance Factor in a Collapsing Fluidized Bed, Chemical Engineering Science 49, 811-819.

Chaouki, J. Chavarie, C. Klvana, D. 1985. Effect of interparticle forces on the hydrodynamic behaviour of fluidized aerogels, Powder Technology 43, 117-125.
Deshpande, V.V. Telang, M.S. 1950. Pipet Method of sedimentation Analysis, Analytical Chemistry 22, 840-841.
Dry, R.J. Judd, M.R. Shingles, T. 1983. Two-Phase Theory and Fine Powders, Powder Technology 34, 213-223.
Geldart, D. 1973. Types of gas fluidization, Powder Technology 7, 285-292.
Geldart, D. Wong, A.C.Y. 1985. Fluidization of Powders Showing degrees of Cohesiveness-II. Experiments on Rates of De-aeration, Chemical Engineering Science 40, 653-661.
Iwadate, Y. Horio, M. 1998. Prediction of agglomerate sizes in bubbling fluidized beds of group C powders, Powder Technology 100, 223-236.
Jeong, S.W. Lee, J.H. Kim, J. Lee, D.H. 2016. Fluidization behaviors of different types of multi-walled carbon nanotubes in gas-solid fluidized beds, Journal of Industrial and Engineering Chemistry 35, 217-223.
Jiang, W. Ding, G. Peng, H. Hu, H. 2010. Modeling of nanoparticles' Aggregation and Sedimentation in Nanofluid, Current Applied Physics 10, 934-941.
Kiani, A. Sotudeh-Gharebagh, R. Mostoufi, N. 2013. Cluster Size Distribution in the Freeboard of a Gas-solid Fluidized Bed, Powder Technology 246, 1-6.
Matsuda, S. Hatano, H. Muramoto, T. Tsutsumi, A. 2004. Modeling for Size Reduction of Agglomerates in Nanoparticle Fluidization, AIChE Journal 50, 2763-2771.
Morooka, S. Kusakabe, K. Kobata, A. Kato, Y. 1988. Fluidization state of ultrafine powders, Journal of Chemical Engineering of Japan 21, 41-46.
Nam, C.H. Pfeffer, R. Dave, R.N. Sundaresan, S. 2004. Aerated vibrofluidization of silica nanoparticles, AIChE Journal 50, 1776-1785.
Smith, J.S. Gardenier JR., R. 1953. Determination of Particle Size Distributions by a Sedimentation method, Analytical Chemistry 25, 577-581.
Park, J.J. Park, J.H. Chang, I.S. Kim, S.D. Choi, C.S. 1991. A New Bed-Collapsing Technique for Measuring the Dense Phase Properties of Gas-Fluidized Beds, Powder Technology 66, 249-257.
Tung, Y. Kwauk, M. 1982. Fluidization-Science and Technology Eds., M. Kwauk and D. kunii, Science Press, Beijing.
Wang, X.S. Palero, V. Soriam, J. Rhodes, M.J. 2006a. Laser-based planar imaging of nano-particle fluidization: Part I – determination of aggregate size and shape, Chemical Engineering Science 61, 5476-5486.
Wang, X.S. Palero, V. Soriam, J. Rhodes, M.J. 2006b. Laser-based planar imaging of nano-particle fluidization: Part II – mechanistic analysis of nanoparticle aggregation, Chemical Engineering Science 61, 8040-8049.
Wang, X.S. Rahman, F. Rhodes, M.J. 2007. Nanoparticle fluidization and Geldart's classification, Chemical Engineering Science 62, 3455-3461.
Wang, Y. Gu, G. Wei, F. Wu, J. 2002. Fluidization and agglomerate structure of SiO2 nanoparticles, Powder Technology 124, 152-159.
Weber, J.M. Mei, J.S. 2013. Bubbling, Bubbling fluidized bed characterization using electrical capacitance volume tomography (ECVT), Powder Technology 242, 40-50.
Yang, Z. Tung, Y. Kwauk, M. 1985. Characterizing Fluidization by the Bed Collapsing Method, Chemical Engineering Communications 39, 217-232.
Yu, H. Zhang, Q. Gu, G. Wang, Y. Luo, G. Wei, F. 2006. Hydrodynamics and gas mixing in a carbon nanotube agglomerate fluidized bed, AIChE Journal 52, 4110-4123.
Yu, H. Zhang, Q. Wei, F. Qian, W. Luo, G. 2003. Agglomerated CNTs synthesized in a fluidized bed reactor: Agglomerate structure and formation mechanism, Carbon, 41, 2855-2863.
Zhou, T. Li, H. 1999. Estimation of agglomerate size for cohesive particles during fluidization, Powder Technology 101, 57-62.
Zhu, C. Yu, Q. Dave, R.N. Pfeffer, R. 2005. Gas fluidization characteristics of nanoparticle agglomerates, AIChE Journal 51, 426-439.
Zhu, J.X. Li, G.Z. Qin, S.Z. Li, F.Y. Zhang, H. Yang, Y.L. 2001. Direct measurements of particle velocities in gas-solids suspension flow using a novel five-fiber optical probe, Powder Technology 115, 184-192.